



Cite this: *Phys. Chem. Chem. Phys.*,
2024, 26, 15292

Elucidating the degradation mechanism of the nerve agent A-234 using various detergents: a theoretical investigation†

Rongxin Shi,^a Lin Zhang,^{ID, a} Denghui Ma^{ab} and Zexing Cao^{ID, *a}

A-234 (ethyl *N*-[1-(diethylamino)ethylidene]phosphoramidofluoridate) is one of the highly toxic Novichok nerve agents, and its efficient degradation is of significant importance. The possible degradation mechanisms of A-234 by H_2O , H_2O_2 , NH_3 , and their combinations have been extensively investigated by using density functional theory (DFT) calculations. According to the initial intermolecular interaction and the proton transfer patterns between the detergent and the substrate A-234, the A-234 degradation reaction is classified into three categories, denoted as A, B, and C. In modes A and B, the degradation of A-234 by H_2O_2 , H_2O , and NH_3 is initiated by the nucleophilic attack of the O or N atom of the detergent on the P atom of A-234, coupled with the proton transfer from the detergent to the O or N atom of A-234, whereas in mode C, the direct interaction of $\text{H}_2\text{N}-\text{H}$ with the F-P bond of A-234 triggers ammonolysis through a one-step mechanism with the formation of H-F and N-P bonds. Perhydrolysis and hydrolysis of A-234 can be remarkably promoted by introducing the auxiliary NH_3 , and the timely formed hydrogen bond network among detergent, auxiliary, and substrate molecules is responsible for the enhancement of degradation efficiency.

Received 29th February 2024,
Accepted 3rd May 2024

DOI: 10.1039/d4cp00881b

rsc.li/pccp

1. Introduction

A-series nerve agents (NAs), also known as Novichok agents, represent a subclass of extremely poisonous organophosphorus compounds, structurally resembling the well-known G-series and V-series nerve agents.^{1–4} Notable for their potency, these NAs have attracted widespread international attention, particularly due to their involvement in high-profile incidents in 2018.⁵ Similar to the G-series and V-series NAs, A-series NAs exert the poisoning effect by inhibiting the activity of acetylcholinesterase (AchE), the enzyme responsible for breaking down acetylcholine. As a result, the accumulation of acetylcholine in synapses occurs, impairing the physiological function of living organisms.⁶ The prolonged presence of NAs in the environment raises apprehensions about long-term consequences, and a comprehensive understanding of

their degradation mechanisms is highly required to develop rapid, convenient and efficient degradation strategies.

Great efforts have been made to decontaminate NAs effectively, both experimentally and theoretically.^{7–27} Metal-organic frameworks (MOFs), leveraging their catalytic properties, have demonstrated that they can facilitate the degradation of NAs.^{7–13} Additionally, various metal oxides, such as MgO , Al_2O_3 , TiO_2 , Cu_2O , CuO , and ZnO , have considerable potential for adsorbing and decomposing NAs.^{14–21} The biodegradation of NAs by enzymes under mild conditions, such as phosphotriesterase (PTE) successfully used in degrading organophosphorus pesticides, has also received considerable interest.^{22–27}

In addition, active detergents were used for detoxification of NAs in the past few decades. For example, hydrogen peroxide (H_2O_2), recognized for its noncorrosive and nonhazardous nature, has shown environmentally friendly behavior in degradation of organophosphorus NAs.^{28–34} H_2O_2 in combination with appropriate activators (*i.e.*, bicarbonate, citrate, and molybdate) may decontaminate nerve agents VX (*O*-ethyl *S*-[2-(diisopropylamino)ethyl]methylphosphonothioate) and GD (pinacolyl methylphosphonofluoridate) through perhydrolysis, resulting in the formation of their non-toxic phosphonates.³⁰ The microporous activated carbons may adsorb these chemical warfare agents, and the adsorbed nerve agents VX, sarin (*O*-isopropyl methylphosphonofluoridate), and HD (bis(2-chloroethyl)sulfide) can be efficiently decomposed by using

^a State Key Laboratory of Physical Chemistry of Solid Surfaces and Fujian Provincial Key Laboratory of Theoretical and Computational Chemistry, College of Chemistry and Chemical Engineering, Xiamen University, Xiamen, 361005, China.

E-mail: zxcao@xmu.edu.cn; Tel: +86-592-2186081

^b School of New Energy, Ningbo University of Technology, Ningbo, 315336, China

† Electronic supplementary information (ESI) available: Additional computational details; predicted relative free energy profiles for A-234 degradation by selected detergents at the M06-2X/6-311++G(d,p)/SMD level of theory; estimated reaction rate constants for selected rate-limiting steps; optimized coordinates of all the discussed species. See DOI: <https://doi.org/10.1039/d4cp00881b>

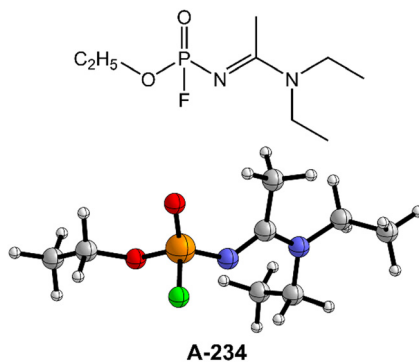


Fig. 1 The molecular structure of A-234.

the hydrogen peroxide solution under ambient conditions, which provides a potentially environmentally friendly approach for the detoxification of adsorbed NAs.³⁵

NAs are highly toxic organophosphates (OPs) and they can be degraded through hydrolysis, and H_2O as a green detergent might be used for decontamination of NAs. However, previous studies showed that the nerve agent did not react with H_2O , and the hydrolysis of VX depends on the pH and temperature.³⁶ In particular, the hydrolytic product of VX from the P–O bond cleavage is almost as toxic as VX in neutral to weakly basic solutions and further detoxification treatment is urgently required. Theoretically, Ramasami and co-workers studied the hydrolysis mechanisms of A-234 using DFT calculations, and the hydrolysis at the acetamidine center is predicted to be more favorable thermodynamically than that at the phosphinate center, leading to the hydrolysis product with the presence of the P–F bond.³⁷ Alternatively, ammonolysis is another potential strategy to degrade NAs.³⁸ Das and co-workers investigated the ammonolysis mechanisms of a nerve agent simulant, *O,S*-dimethyl methylphosphonothiolate (DMPT), using DFT calculations and molecular dynamics simulations, the stepwise degradation pathway is predicted to be more favorable than the concerted one, and NH_3 as the catalyst can effectively reduce the activation energy of the stepwise reaction.³⁹ Besides, Mandal compared the decontamination of nerve agent tabun ([dimethylamino(ethoxy)phosphoryl]formonitrile) by using NH_3 and H_2O , based on DFT and MP2 calculations, and the former is a more efficient degradation reagent.⁴⁰

Despite such considerable efforts to deal with the G- and V-series NAs, the knowledge of Novichok agents is still quite limited even now.^{12,37,41} The existing literature data of A-series NAs primarily focus on their structural and spectroscopic properties from theoretical calculations and mass spectrometric studies.^{42–45} Note that the perhydrolysis mechanism of A-series NAs by H_2O_2 and the ammonolysis mechanism of A-series NAs by NH_3 are still not well-understood to the best of our knowledge. Herein, the degradation of Novichok agent A-234, one of the A-series NAs as shown in Fig. 1, has been explored by extensive DFT calculations, and the differences in the degradation mechanism and efficiency by H_2O , H_2O_2 , and NH_3 were discussed. Furthermore, the detoxification performances of different detergent combinations (such as $\text{H}_2\text{O}_2/\text{H}_2\text{O}$, $\text{H}_2\text{O}_2/\text{NH}_3$, $\text{H}_2\text{O}/\text{H}_2\text{O}_2$, and $\text{H}_2\text{O}/\text{NH}_3$, where the

former serves as the nucleophile and the latter serves as a proton donor in these combinations) toward A-234 have been compared.

2. Computational details

All calculations were carried out using the Gaussian 16 program.⁴⁶ Geometric optimizations were performed at the M06-2X⁴⁷/6-311++G(d,p)^{48–52} level of theory. The vibrational analysis at the same level was used to confirm the optimized local minima without an imaginary frequency and the transition-state structures with only one imaginary frequency. Furthermore, all transition states were confirmed to connect corresponding reactants and products by the intrinsic reaction coordinate (IRC) calculations.⁵³ Single-point energy calculations with the implicit solvation model based on density (SMD)⁵⁴ for the solvent water were carried out at the M06-2X/6-311++G(d,p)/SMD level of theory. Different DFT functionals (e.g., M06-2X-D3,⁵⁵ B3LYP,⁵⁶ PBE0,⁵⁷ MN15,⁵⁸ and ω B97X-D⁵⁹) and basis sets (e.g., 6-311++G(2d,2p)^{48–52} and def2-TZVP⁶⁰) were considered, but no qualitatively different results were found (see Tables S1 and S2 in the ESI†). Unless otherwise stated, here all the thermochemical properties were discussed based on the predicted results at the M06-2X/6-311++G(d,p)/SMD//M06-2X/6-311++G(d,p) level of theory under the standard conditions (298.15 K and 1 atm). Fig. S1–S3 (ESI†) show the predicted relative free energy profiles for the degradation of A-234 by H_2O_2 , H_2O , and NH_3 , based on the gas-phase optimized structures and vibrational frequencies combined with the single-point energy calculation including the solvent effect, showing good agreement with those obtained through M06-2X/6-311++G(d,p)/SMD geometry optimizations and vibrational frequency analyses, and similarly, their corresponding equilibrium geometries of the species involved in the reaction are of good consistency. All the geometric structures are visualized by using CYLview.⁶¹

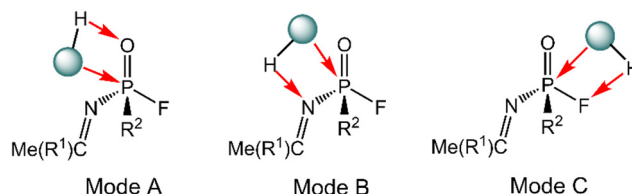
3. Results and discussion

3.1 A-234 degradation using different detergents

The degradation mechanism of A-234 by H_2O_2 , H_2O , and NH_3 was examined first. At the initial stage of the reaction, the nucleophilic attack of O atoms for H_2O and H_2O_2 or the N atom for NH_3 on the P center of A-234 was considered. During this

■ = O (for H_2O_2 and H_2O); and N (for NH_3)

$\text{R}^1 = \text{N}(\text{Et})_2$, $\text{R}^2 = \text{OEt}$



Scheme 1 Plausible modes for the nucleophilic attack of H_2O_2 , H_2O , and NH_3 on A-234.

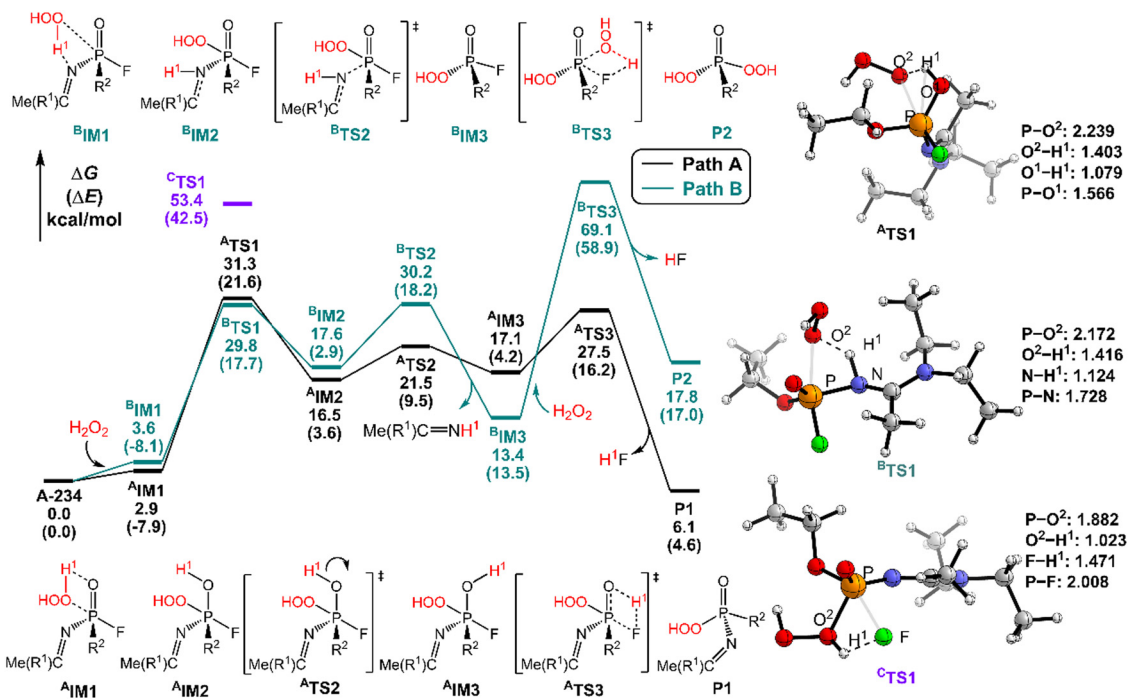


Fig. 2 Predicted relative free energy profiles (ΔG in kcal mol^{-1}) and electronic energies (ΔE in parentheses) of the species involved in the perhydrolysis of A-234 by H_2O_2 . The main transition state structures and the selected key bond lengths (in \AA) are given.

process, protons from the detergents may be transferred to different atomic sites in A-234, resulting in various degradation products. Accordingly, we categorize the degradation process triggered by the nucleophilic attack of the detergent on A-234 into three reaction modes A, B, and C (see Scheme 1), where protons were transferred to the O, N, and F atoms of A-234, respectively.

3.1.1 A-234 perhydrolysis by H_2O_2 . The perhydrolysis mechanism of A-234 by H_2O_2 is depicted in Fig. 2. Notably, the three nucleophilic attack modes of H_2O_2 on A-234 initiate different reaction pathways, and the predicted relative energies of the stationary points along the reaction pathway are referenced to A-234 and H_2O_2 .

The perhydrolysis of A-234 by H_2O_2 through path A begins with the formation of the molecular complex ^AIM1, where the $\text{HOO}-\text{H}^1\cdots\text{O}=\text{P}$ hydrogen bond interaction stabilizes ^AIM1. The nucleophilic attack of the O atom in H_2O_2 on the P atom of A-234, coupled with the proton transfer (H^1) from H_2O_2 to the O atom of A-234, leads to a metastable intermediate ^AIM2 through the transition state ^ATS1 with a free energy barrier of 28.4 kcal mol^{-1} . Subsequently, ^AIM2 evolves into ^AIM3 through rotation of the $\text{P}-\text{OH}^1$ moiety with a low free energy barrier of 5.0 kcal mol^{-1} , in which H^1 and F atoms are in the same side of P-O. Followed by the coupling of H^1 and F atoms in ^AIM3 and the release of HF, the degradation product ^P1 is formed through a four-membered ring transition state ^ATS3 with a free energy barrier of 10.4 kcal mol^{-1} . The degradation path A is an endergonic process with a Gibbs free energy of the reaction ΔG of 6.1 kcal mol^{-1} .

Similar to the path A above, here path B also initiates from a molecular complex ^BIM1, where the $\text{HOO}-\text{H}^1\cdots\text{N}-(\text{A}-234)$

hydrogen bond interaction is involved in ^BIM1, differing from ^AIM1. Afterwards, the H^1 is transferred to the N atom coupled with the nucleophilic attack of the O atom of H_2O_2 on the P center of A-234 yielding a metastable ^BIM2 through a four-membered ring transition state ^BTS1 with a free energy barrier of 26.2 kcal mol^{-1} . The cleavage of the P-N bond in ^BIM2, coupled with the release of $\text{Me}(\text{R}^1)\text{C}=\text{NH}$, produces an intermediate ^BIM3 via ^BTS2 with a free energy barrier of 12.4 kcal mol^{-1} . Note that ^BIM3 may be toxic owing to the presence of P-F, and thus it needs to be further detoxicated by an additional H_2O_2 molecule. However, the cleavage of the P-F bond in ^BIM3 experiences a substantially high free energy barrier of 55.7 kcal mol^{-1} , suggesting that ^BIM3 could be the end-product of path B. Path B from A-234 to ^BIM3 is also a thermodynamically endergonic process with a Gibbs free energy of the reaction ΔG of 13.4 kcal mol^{-1} . Although both paths A and B may compete with each other at the initial stage, overall, path A is more favorable for the perhydrolysis of A-234 by H_2O_2 , both kinetically and thermodynamically, compared to path B.

The path C for the perhydrolysis of A-234 by H_2O_2 involves the four-membered ring transition state ^CTS1, where the H^1 of H_2O_2 is transferred to the F site coupled with the nucleophilic attack of the O atom of H_2O_2 on the P atom of A-234, with a substantially high free energy barrier of 53.4 kcal mol^{-1} . Therefore, such a direct activation mode of the P-F bond is considered unfavorable. Clearly, path A is inevitably responsible for the perhydrolysis of A-234 during its degradation by H_2O_2 .

3.1.2 A-234 hydrolysis by H_2O . The hydrolysis of A-234 by H_2O has been further investigated, and the degradation follows the mechanism similar to that by H_2O_2 , as shown in Fig. 3.

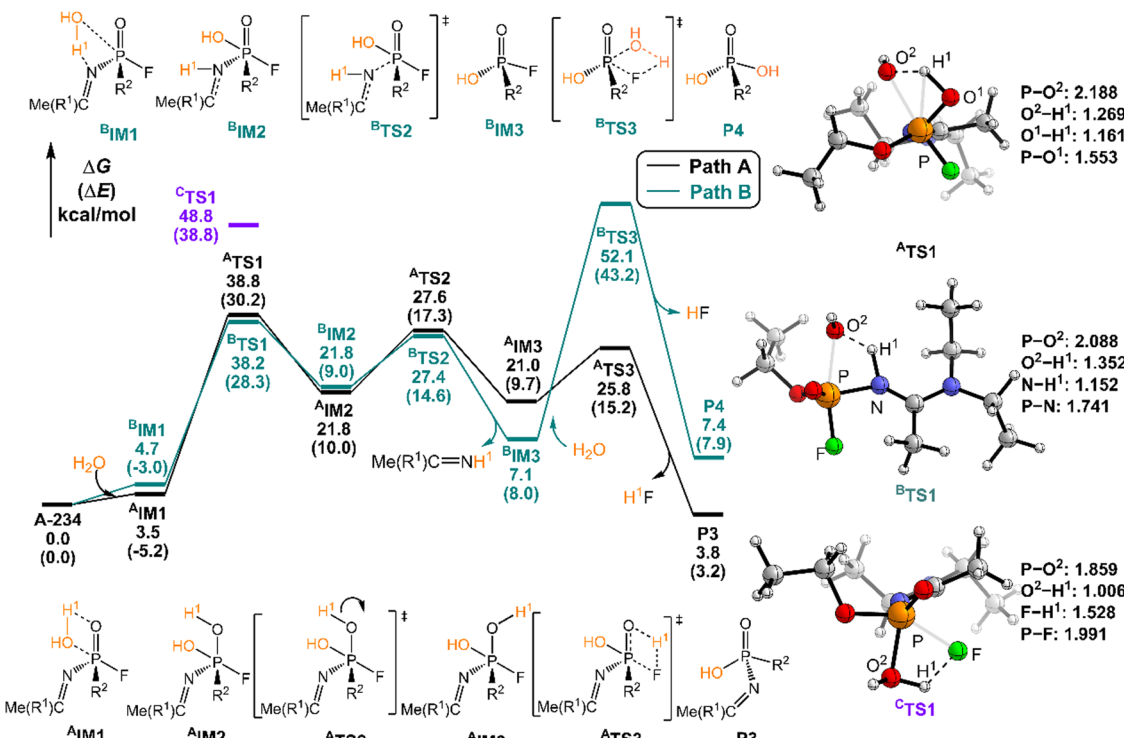


Fig. 3 Predicted relative free energy profiles (ΔG in kcal mol⁻¹) and electronic energies (ΔE in parentheses) of the species involved in the hydrolysis of A-234 by H_2O . The main transition state structures and the selected key bond lengths (in Å) are given.

Similarly, the three nucleophilic attack modes of H_2O on A-234 induced three different reaction pathways, and the predicted

relative energies of the species involved in the reaction pathway are referenced to A-234 and H_2O .

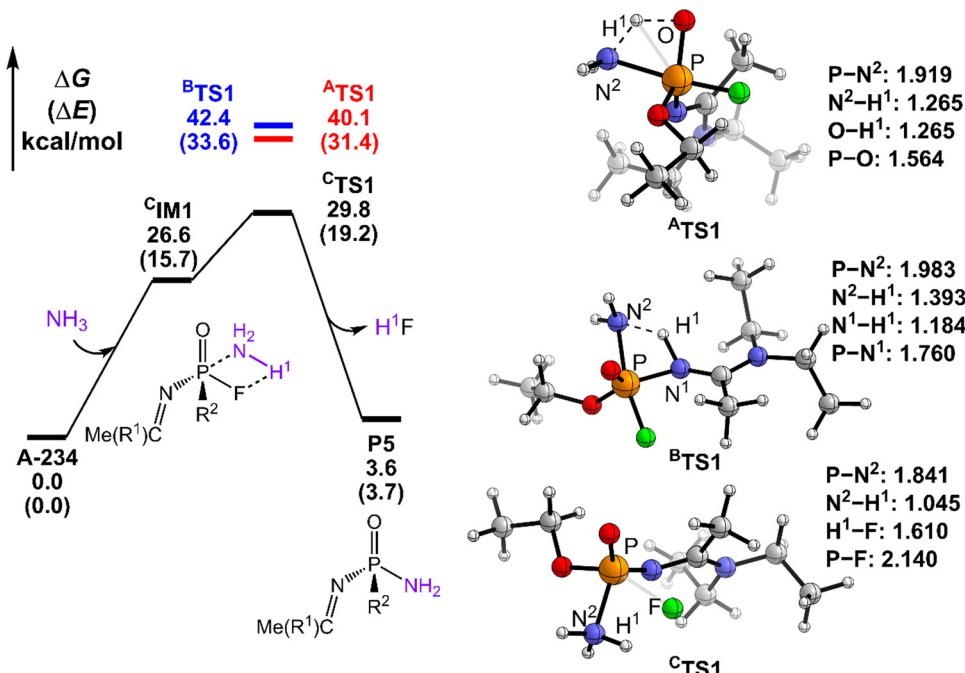


Fig. 4 Predicted relative free energy profiles (ΔG in kcal mol⁻¹) and electronic energies (ΔE in parentheses) of the species involved in the ammonolysis of A-234 by NH_3 , where for paths A and B, only the key transition states are shown in red and blue, respectively. The main transition state structures and the selected key bond lengths (in Å) are given.

In path A, the hydrolysis of A-234 by H_2O starts from the generation of a molecular complex ${}^A\text{IM1}$ derived from a hydrogen bond interaction between the H^1 atom of H_2O and the $\text{P}=\text{O}$ moiety of A-234. Then, the proton H^1 shifts to the O atom of the $\text{P}=\text{O}$ moiety, coupled with the nucleophilic attack of the newly generated HO^- on the P atom, leading to a metastable intermediate ${}^A\text{IM2}$ *via* ${}^A\text{TS1}$ with a free energy barrier of 35.2 kcal mol⁻¹. Afterwards, the rotation of the $-\text{P}-\text{OH}^1$ bond in ${}^A\text{IM2}$ leads to the formation of ${}^A\text{IM3}$ through ${}^A\text{TS2}$ with a low free energy barrier of 5.8 kcal mol⁻¹. This isomerization process reduces the distance between H^1 and F atoms and boosts the elimination of the F atom in the form of HF. Followed by the formation of the H^1F molecule through a four-membered ring transition state ${}^A\text{TS3}$ with a free energy barrier of 4.8 kcal mol⁻¹, the degradation product P3 is obtained. The path A for the A-234 hydrolysis by H_2O has a Gibbs free energy of the reaction ΔG of 3.8 kcal mol⁻¹.

In path B, the molecular complex ${}^B\text{IM1}$ with H_2O with A-234 is formed first through the $\text{HO}-\text{H}\cdots\text{N}-(\text{A}-234)$ hydrogen bond interaction. Subsequently, the nucleophilic attack of the O atom of H_2O on the P atom, coupled with the proton H^1 shift to the N atom, yields a metastable intermediate ${}^B\text{IM2}$ through ${}^B\text{TS1}$ with a free energy barrier of 33.5 kcal mol⁻¹. Note that the P-N bond in ${}^B\text{IM2}$ is remarkably stretched and weakened. With the leaving of the $\text{Me}(\text{R}^1)\text{C}=\text{NH}$ species, an intermediate ${}^B\text{IM3}$ is formed through ${}^B\text{TS2}$ with a free energy barrier of

5.6 kcal mol⁻¹. The hydrolytic breakage of the P-F bond in ${}^B\text{IM3}$ by additional H_2O , coupled with the release of HF, generates the degraded product P4 through the four-membered transition state ${}^B\text{TS3}$ with a relatively high free energy barrier of 45.0 kcal mol⁻¹. Similar to the perhydrolysis of A-234 in Fig. 2, the hydrolysis of A-234 through path B is also an unfavorable process, both kinetically and thermodynamically, compared to path A.

In the hydrolysis path C of A-234 by H_2O , H_2O approaches A-234 from the direction of the P-F bond first. The subsequent degradation experiences ${}^C\text{TS1}$ with a substantially high free energy barrier of 48.8 kcal mol⁻¹, and the proton H^1 transfer from H_2O to the F atom site of A-234, along with the nucleophilic attack of the O atom of H_2O on the P atom of A-234, is involved in the hydrolysis process. Clearly, both paths B and C are less possible for the A-234 hydrolysis.

3.1.3 A-234 ammonolysis by NH_3 . As shown in Fig. 4, the ammonolysis mechanisms of A-234 by NH_3 have been investigated, and the calculated results indicate that the free energy barrier values for paths A, B, and C are 40.1, 42.4, and 29.8 kcal mol⁻¹, respectively. Therefore, path C is the most favorable ammonolysis mechanism energetically, differing from the perhydrolysis and hydrolysis of A-234.

Here, the path preference for A-234 degradation by NH_3 can be ascribed to the relatively stronger electron-donating ability of NH_3 as a weak proton donor than that of H_2O_2 or H_2O ,

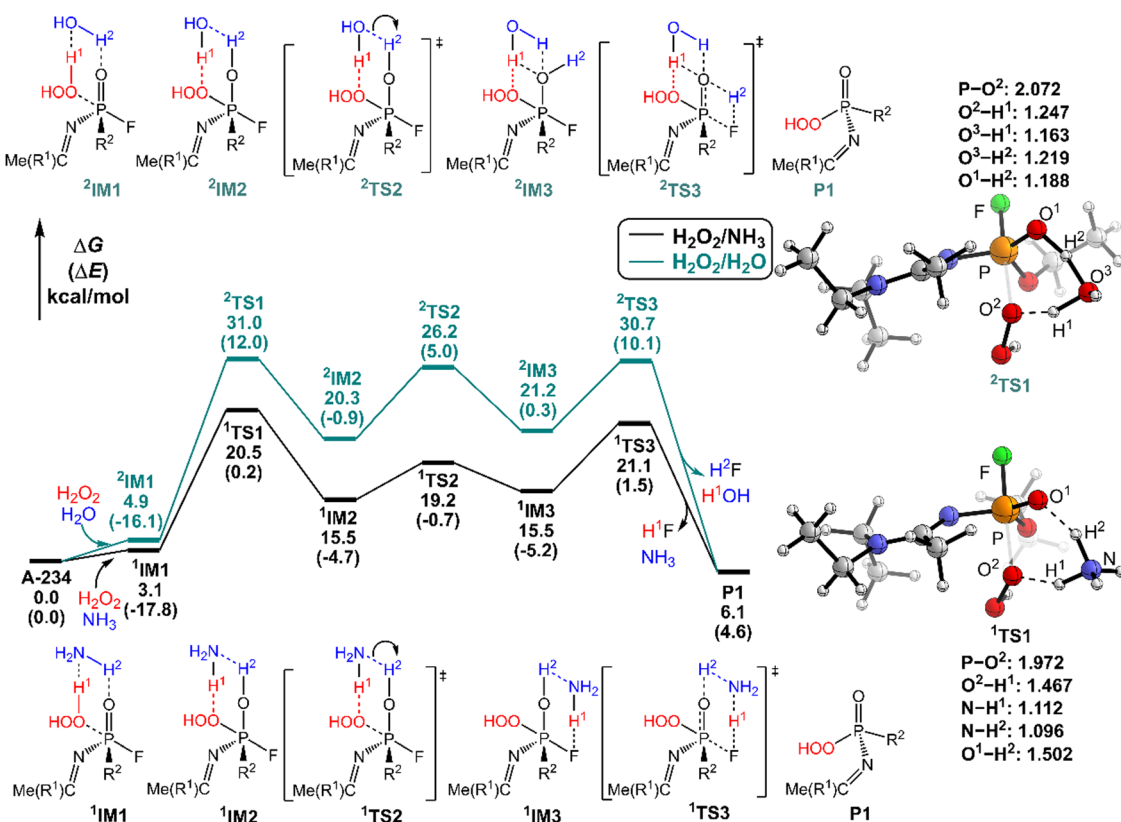


Fig. 5 Predicted relative free energy profiles (ΔG in kcal mol⁻¹) and electronic energies (ΔE in parentheses) of the species involved in the perhydrolysis of A-234 by $\text{H}_2\text{O}_2/\text{NH}_3$ and $\text{H}_2\text{O}_2/\text{H}_2\text{O}$. The main transition state structures and the selected key bond lengths (in Å) are given.

resulting in that the nucleophilic attack of NH_3 on the P center of A-234 (path C) is favored. Such superiority of path C is also supported by further IRC analyses related to the key transition states ($^4\text{TS1}$, $^3\text{TS1}$, and $^2\text{TS1}$) in the perhydrolysis and ammonolysis of A-234. For $^4\text{TS1}$ and $^3\text{TS1}$ in paths A and B, their energy demands are mainly caused by the proton transfer process from the detergents (H_2O_2 and NH_3) to A-234, suggesting that both paths A and B are dominated by the proton transfer step (see Fig. S4a and b and d and e in the ESI[†]). However, for $^2\text{TS1}$ in path C (Fig. S4c and f, ESI[†]), its energy requirement primarily arises from the cleavage of the P–F bond, along with the proton transfer from the detergent to the F atom of A-234, which can be facilitated by the nucleophilic attack of NH_3 on the P center of A-234. Overall, the relatively strong proton-donating ability of H_2O_2 (or H_2O), than that of NH_3 , may facilitate the perhydrolysis (or hydrolysis) of A-234 through paths A and B, while the ammonolysis of A-234 by NH_3 primarily proceeds *via* path C owing to the stronger nucleophilicity of NH_3 than those of H_2O_2 and H_2O .

Overall, the perhydrolysis and hydrolysis of A-234 generally follow path A with relatively low free energy spans and thermodynamically comparative advantages, although path B is competitive at the initial stage of the A-234 degradation. However, the ammonolysis of A-234 is dominated by path C. Notably, the direct degradation of A-234 respectively by using H_2O_2 , H_2O , or NH_3 experiences relatively high free energy barriers, and thus

its efficient degradation requires harsh reaction conditions and the optimal combination of detergents or catalysts.

3.2 A-234 degradation by different combinations of detergents

It was found that the mixture of H_2O_2 vapor with NH_3 gas could degrade the nerve agent VX on solid surfaces at ambient temperature, indicating that the notable combination effect of H_2O_2 with NH_3 toward the decontamination of VX.⁶² Speculatively, the hydrogen bonding networks formed by the detergents themselves or with solvent molecules exist in the admixture, which may play a crucial role in promoting the degradation of NAs. Therefore, further computational efforts are made to elucidate the combination effects of different detergents (*e.g.*, $\text{H}_2\text{O}_2/\text{H}_2\text{O}$, $\text{H}_2\text{O}_2/\text{NH}_3$, $\text{H}_2\text{O}/\text{H}_2\text{O}$, and $\text{H}_2\text{O}/\text{NH}_3$) on the degradation efficiency of A-234. In these combinations, the former serves as the nucleophilic reagent and the latter as an auxiliary agent to donate the proton.

The predicted degradation mechanisms and relative energies of A-234 by detergent combinations of $\text{H}_2\text{O}_2/\text{NH}_3$ and $\text{H}_2\text{O}_2/\text{H}_2\text{O}$ are shown in Fig. 5. The degradation of A-234 by $\text{H}_2\text{O}_2/\text{NH}_3$ through path A commences with the formation of the molecular complex $^4\text{IM1}$, where a novel hydrogen bond network is involved in $^4\text{IM1}$. The hydrogen bond interaction plays a crucial role in facilitating the subsequent proton transfer. The proton transfers from H_2O_2 to the N atom of NH_3 (H^1) and simultaneously from

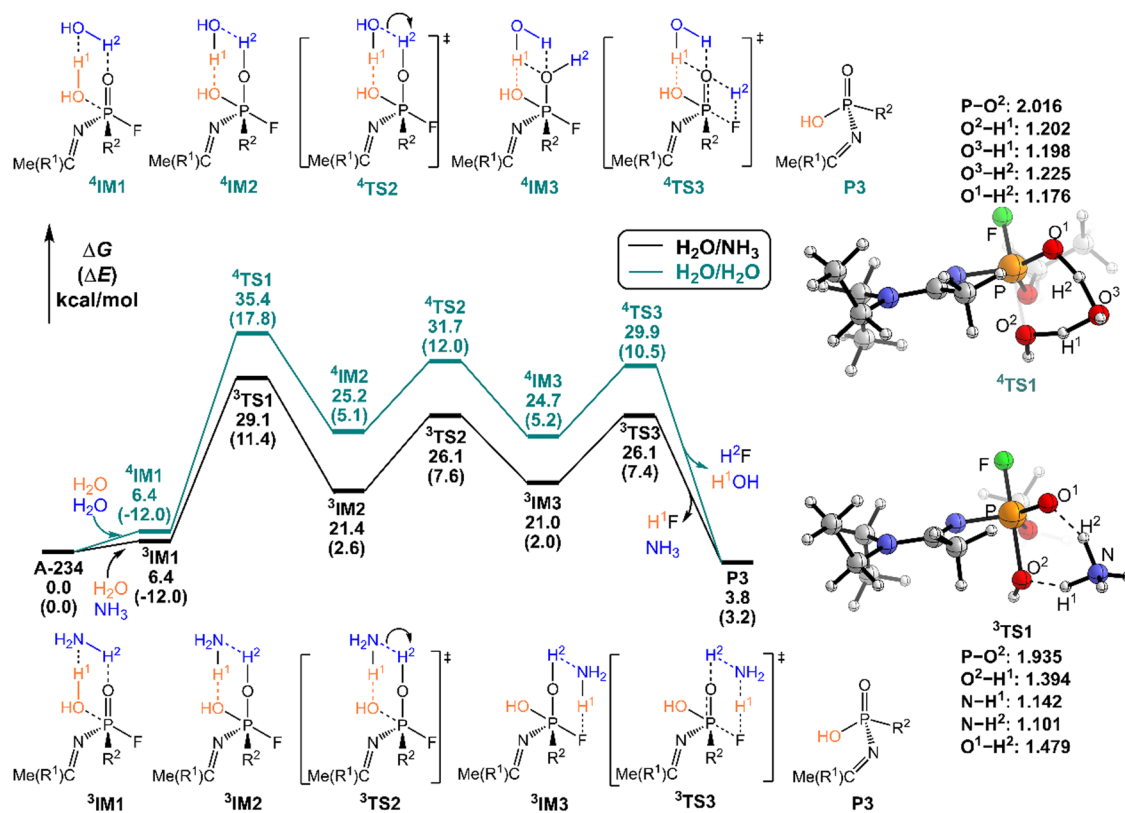


Fig. 6 Predicted relative free energy profiles (ΔG in kcal mol^{-1}) and electronic energies (ΔE in parentheses) of the species involved in the hydrolysis of A-234 by $\text{H}_2\text{O}/\text{NH}_3$ and $\text{H}_2\text{O}/\text{H}_2\text{O}$. The main transition state structures and the selected key bond lengths (in Å) are given.

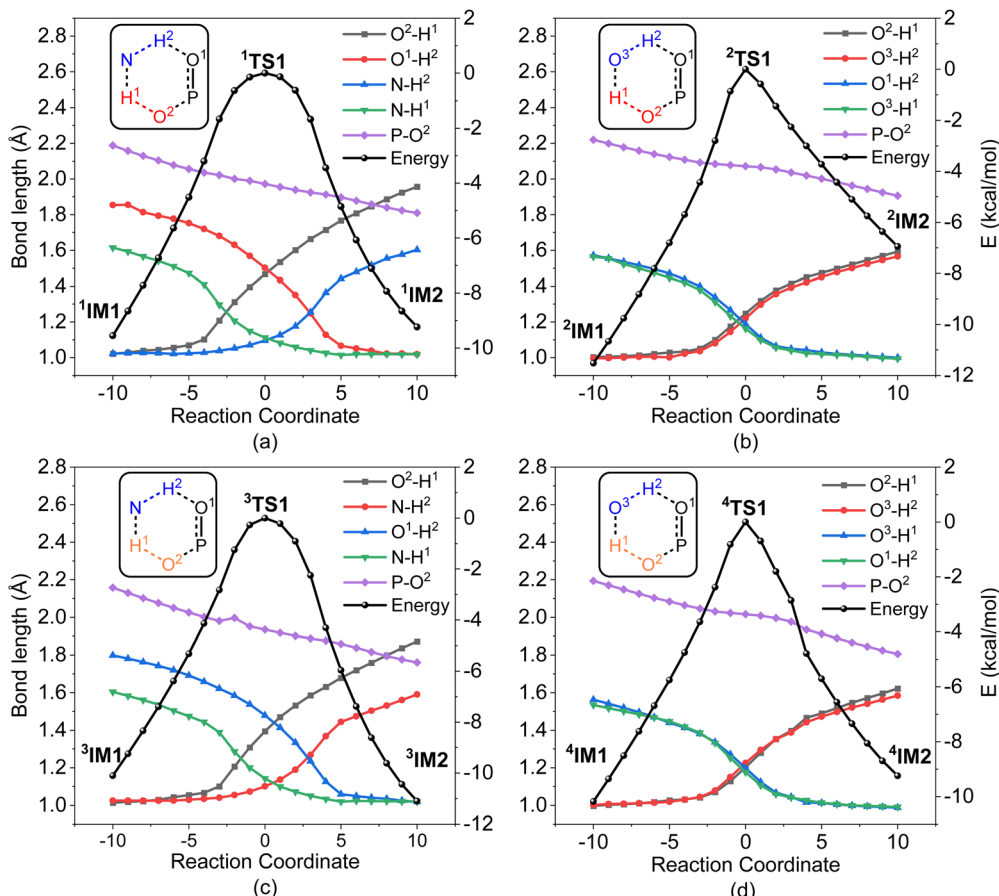


Fig. 7 IRC analysis for the key transition states: (a) $^1\text{TS1}$ for $\text{H}_2\text{O}_2/\text{NH}_3$, (b) $^2\text{TS1}$ for $\text{H}_2\text{O}_2/\text{H}_2\text{O}$, (c) $^3\text{TS1}$ for $\text{H}_2\text{O}/\text{NH}_3$, and (d) $^4\text{TS1}$ for $\text{H}_2\text{O}/\text{H}_2\text{O}$.

NH_3 to the O atom in the $\text{P}=\text{O}$ moiety (H^2) mediated by the hydrogen bond network, coupled with the nucleophilic attack of the resulting HOO^- anion to the P atom of A-234, lead to the formation of the metastable $^1\text{IM2}$ via a six-membered ring $^1\text{TS1}$ with a free energy barrier of $17.4 \text{ kcal mol}^{-1}$. $^1\text{IM2}$ evolves into the isoenergetic isomer $^1\text{IM3}$ through the rotation of the $-\text{P}-\text{OH}^2$ bond with a low free energy barrier of $3.7 \text{ kcal mol}^{-1}$, where the hydrogen bond network may facilitate the coupling of H^1 and F atoms. Finally, the rebound of H^2 to the NH_2 moiety to regenerate NH_3 , coupled with the formation and release of HF, yields the nontoxic **P1** through a six-membered ring $^1\text{TS3}$ with a free energy barrier of $5.6 \text{ kcal mol}^{-1}$. Fig. 2 and 5 show that the free energy barrier of the nucleophilic attack in the degradation of A-234 remarkably decreases from $31.3 \text{ kcal mol}^{-1}$ by H_2O_2 (or $31.0 \text{ kcal mol}^{-1}$ by $\text{H}_2\text{O}_2/\text{H}_2\text{O}$) to $20.5 \text{ kcal mol}^{-1}$ by $\text{H}_2\text{O}_2/\text{NH}_3$. Here, the presence of NH_3 constitutes a hydrogen bonding network to mediate the hydrogen transfer, which enhances the degradation efficiency of H_2O_2 toward A-234.

The degradation of A-234 by $\text{H}_2\text{O}_2/\text{H}_2\text{O}$ with the H_2O as the auxiliary agent was also investigated, and the corresponding results are shown in Fig. 5. Note that the degradation of A-234 by $\text{H}_2\text{O}_2/\text{H}_2\text{O}$ takes place on a higher free-energy surface than that by $\text{H}_2\text{O}_2/\text{NH}_3$, suggesting that NH_3 should be a better auxiliary agent than H_2O .

As shown in Fig. 6, the degradation mechanisms of A-234 by $\text{H}_2\text{O}/\text{NH}_3$ and $\text{H}_2\text{O}/\text{H}_2\text{O}$ were investigated. Compared to the

hydrolysis of A-234 using a single molecule of H_2O , the presence of NH_3 or additional H_2O significantly increases the degradation efficiency of H_2O toward A-234. Particularly, NH_3 as the prodegradant is superior to H_2O , and the free energy barrier of the rate-determining step in the degradation of A-234 is remarkably reduced from $38.8 \text{ kcal mol}^{-1}$ by H_2O to $29.1 \text{ kcal mol}^{-1}$ by $\text{H}_2\text{O}/\text{NH}_3$.

In order to gain an insight into the difference in detoxification efficiency for H_2O_2 and H_2O , as well as the effects of auxiliary agents NH_3 and H_2O on the degradation of A-234, IRC analysis has been performed on the key transition states, including $^1\text{TS1}$, $^2\text{TS1}$, $^3\text{TS1}$ and $^4\text{TS1}$. As shown in Fig. 7a and c, the hydrogen transfers from O^2 to $\text{N}(\text{H}^1)$ and from N to $\text{O}^1(\text{H}^2)$ in both $^1\text{TS1}$ and $^3\text{TS1}$ are concerted but not synchronous, which may be ascribed to different hydrogen bonds $\text{O}-\text{H}\cdots\text{N}$ and $\text{N}-\text{H}\cdots\text{O}$ that are involved in the concerted proton transfer of perhydrolysis and hydrolysis assisted by NH_3 . The presence of NH_3 facilitates the proton transfer and the formation of strong nucleophiles HOO^- and HO^- , thereby promoting the degradation of A-234 by H_2O_2 and H_2O . In contrast, during the degradation process assisted by H_2O , the proton transfers in $^2\text{TS1}$ and $^4\text{TS1}$ are concerted and synchronous, owing to the involvement of same hydrogen-bond networks. Additionally, the higher basicity of NH_3 , than that of H_2O ,⁶³ renders it more receptive to the proton from H_2O_2 or H_2O , further facilitating

the formation of strong nucleophiles and thereby promoting the degradation process.

Furthermore, regardless of the presence of an auxiliary agent, the degradation efficiency of H_2O_2 toward A-234 is higher than that of H_2O , which is attributed to the superior proton-donating capacity of H_2O_2 , than that of H_2O , as evidenced by their respective $\text{p}K_a$ values (11.6 for H_2O_2 and 14.0 for H_2O).⁶³

4. Conclusions

Here, the plausible degradation mechanisms of A-234 by H_2O_2 , H_2O , NH_3 and their combinations were investigated by using DFT calculations. The calculated results revealed that the degradation of A-234 by H_2O_2 and H_2O is triggered by the nucleophilic attack on the P center of A-234 coupling with the proton transfer to the O atom of the $\text{P}=\text{O}$ moiety *via* path A, while $\text{H}_2\text{N}-\text{H}$ and $\text{F}-\text{P}-(\text{A}-234)$ tend to interact directly in the ammonolysis of A-234 by NH_3 *via* path C. Both H_2O_2 and NH_3 have relatively high degradation efficiency toward A-234 than H_2O . More importantly, various combinations of detergents (nucleophile/auxiliary: $\text{H}_2\text{O}_2/\text{H}_2\text{O}$, $\text{H}_2\text{O}_2/\text{NH}_3$, $\text{H}_2\text{O}/\text{H}_2\text{O}$, and $\text{H}_2\text{O}/\text{NH}_3$) may remarkably promote the degradation of A-234, since the hydrogen bond networks among the detergent, auxiliary, and substrate molecules facilitate the initial proton transfers and the formation of strong nucleophiles. In particular, the perhydrolysis and hydrolysis efficiency of A-234 by H_2O_2 and H_2O can be notably improved with the help of NH_3 , suggesting that NH_3 is a better auxiliary agent than H_2O , and this is attributed to the higher basicity of NH_3 to promote the proton transfer than that of H_2O . Furthermore, the degradation of A-234 and the rate-determining step depend on the auxiliary agent. The present findings provide an in-depth understanding of the degradation of A-234 using small-molecule detergents, which is beneficial to the development of effective decontaminants toward the detoxification of A-series nerve agents.

Conflicts of interest

The authors declare that the research was conducted in the absence of any commercial or financial relationships that could be construed as a potential conflict of interest.

Acknowledgements

This work was supported by the National Natural Science Foundation of China (21933009 and 22373078).

References

- 1 S. Costanzi, J.-H. Machado and M. Mitchell, *ACS Chem. Neurosci.*, 2018, **9**, 873–885.
- 2 S. Mukherjee and R. D. Gupta, *J. Toxicol.*, 2020, **2020**, 3007984.
- 3 F. R. Sidell and J. Borak, *Ann. Emerg. Med.*, 1992, **21**, 865–871.
- 4 S. W. Wiener and R. S. Hoffman, *J. Intensive Care Med.*, 2004, **19**, 22–37.
- 5 R. Stone, *Science*, 2018, **359**, 1314–1315.
- 6 B. Sanson, F. Nachon, J.-P. Colletier, M.-T. Froment, L. Toker, H. M. Greenblatt, J. L. Sussman, Y. Ashani, P. Masson, I. Silman and M. Weik, *J. Med. Chem.*, 2009, **52**, 7593–7603.
- 7 Y. Liu, S.-Y. Moon, J. T. Hupp and O. K. Farha, *ACS Nano*, 2015, **9**, 12358–12364.
- 8 J. E. Mondloch, M. J. Katz, W. C. Isley Iii, P. Ghosh, P. Liao, W. Bury, G. W. Wagner, M. G. Hall, J. B. DeCoste and G. W. Peterson, *Nat. Mater.*, 2015, **14**, 512–516.
- 9 P. Li, S.-Y. Moon, M. A. Guelta, L. Lin, D. A. Gómez-Gualdrón, R. Q. Snurr, S. P. Harvey, J. T. Hupp and O. K. Farha, *ACS Nano*, 2016, **10**, 9174–9182.
- 10 N. S. Bobbitt, M. L. Mendonca, A. J. Howarth, T. Islamoglu, J. T. Hupp, O. K. Farha and R. Q. Snurr, *Chem. Soc. Rev.*, 2017, **46**, 3357–3385.
- 11 M. L. Mendonca and R. Q. Snurr, *ACS Catal.*, 2020, **10**, 1310–1323.
- 12 M. C. de Koning, C. Vieira Soares, M. van Grol, R. P. T. Bross and G. Maurin, *ACS Appl. Mater. Interfaces*, 2022, **14**, 9222–9230.
- 13 D. Ma and Z. Cao, *J. Phys. Chem. C*, 2022, **126**, 19159–19168.
- 14 A. Michalkova, L. Gorb, M. Ilchenko, O. A. Zhikol, O. V. Shishkin and J. Leszczynski, *J. Phys. Chem. B*, 2004, **108**, 1918–1930.
- 15 A. Michalkova, M. Ilchenko, L. Gorb and J. Leszczynski, *J. Phys. Chem. B*, 2004, **108**, 5294–5303.
- 16 A. Michalkova, J. Martinez, O. A. Zhikol, L. Gorb, O. V. Shishkin, D. Leszczynska and J. Leszczynski, *J. Phys. Chem. B*, 2006, **110**, 21175–21183.
- 17 V. M. Bermudez, *J. Phys. Chem. C*, 2007, **111**, 3719–3728.
- 18 V. M. Bermudez, *J. Phys. Chem. C*, 2009, **113**, 1917–1930.
- 19 N. Q. Le, C. E. Ekuma, B. I. Dunlap and D. Gunlycke, *J. Phys. Chem. C*, 2018, **122**, 2832–2839.
- 20 R. Tyshevsky, S. Holdren, B. W. Eichhorn, M. R. Zachariah and M. M. Kuklja, *J. Phys. Chem. C*, 2019, **123**, 26432–26441.
- 21 D. Ma and Z. Cao, *J. Phys. Chem. C*, 2021, **125**, 24396–24405.
- 22 V. K. Rastogi, J. J. Defrank, T.-C. Cheng and J. R. Wild, *Biochem. Biophys. Res. Commun.*, 1997, **241**, 294–296.
- 23 K. E. LeJeune, J. R. Wild and A. J. Russell, *Nature*, 1998, **395**, 27–28.
- 24 P.-C. Tsai, A. Bigley, Y. Li, E. Ghanem, C. L. Cadieux, S. A. Kasten, T. E. Reeves, D. M. Cerasoli and F. M. Raushel, *Biochemistry*, 2010, **49**, 7978–7987.
- 25 A. N. Bigley and F. M. Raushel, *Chem.-Biol. Interact.*, 2019, **308**, 80–88.
- 26 F. Fan, Y. Zheng, Y. Zhang, H. Zheng, J. Zhong and Z. Cao, *ACS Catal.*, 2019, **9**, 7038–7051.
- 27 J. Yu, Y. Fu and Z. Cao, *J. Phys. Chem. B*, 2023, **127**, 7462–7471.
- 28 A. M. McAnoy, J. Williams, M. R. L. Paine, M. L. Rogers and S. J. Blanksby, *J. Org. Chem.*, 2009, **74**, 9319–9327.
- 29 E. V. Patterson and C. J. Cramer, *J. Phys. Org. Chem.*, 1998, **11**, 232–240.

30 G. W. Wagner, *Main Group Chem.*, 2010, **9**, 257–263.

31 G. W. Wagner, L. R. Procell, D. C. Sorrick, G. E. Lawson, C. M. Wells, C. M. Reynolds, D. B. Ringelberg, K. L. Foley, G. J. Lumetta and D. L. Blanchard, Jr., *Ind. Eng. Chem. Res.*, 2010, **49**, 3099–3105.

32 G. W. Wagner and Y.-C. Yang, *Ind. Eng. Chem. Res.*, 2002, **41**, 1925–1928.

33 Y.-C. Yang, F. J. Berg, L. L. Szafraniec, W. T. Beaudry, C. A. Bunton and A. Kumar, *J. Chem. Soc., Perkin Trans. 2*, 1997, 607–614.

34 Y. C. Yang, L. L. Szafraniec, W. T. Beaudry and C. A. Bunton, *J. Org. Chem.*, 1993, **58**, 6964–6965.

35 R. Osovsky, D. Kaplan, I. Nir, H. Rotter, S. Elisha and I. Columbus, *Environ. Sci. Technol.*, 2014, **48**, 10912–10918.

36 Y.-C. Yang, *Acc. Chem. Res.*, 1999, **32**, 109–115.

37 Y. A. Imrit, H. Bhakhoa, T. Sergeieva, S. Danés, N. Savoo, M. I. Elzagheid, L. Rhyman, D. M. Andrada and P. Ramasami, *RSC Adv.*, 2020, **10**, 27884–27893.

38 C. J. Leverant, C. W. Priest, J. A. Greathouse, M. K. Kinnan and S. B. Rempe, *Int. J. Mol. Sci.*, 2021, **22**, 8653.

39 D. Mandal, K. Sen and A. K. Das, *J. Phys. Chem. A*, 2012, **116**, 8382–8396.

40 D. Mandal, *Theor. Chem. Acc.*, 2020, **139**, 169.

41 I. Lyagin and E. Efremenko, *Catal. Commun.*, 2019, **120**, 91–94.

42 H. Bhakhoa, L. Rhyman and P. Ramasami, *R. Soc. Open Sci.*, 2019, **6**, 181831.

43 S. E. Hosseini, H. Saeidian, A. Amozadeh, M. T. Naseri and M. Babri, *Rapid Commun. Mass Spectrom.*, 2016, **30**, 2585–2593.

44 K. Jeong and J. Choi, *R. Soc. Open Sci.*, 2019, **6**, 190414.

45 L. A. Vieira, J. S. F. D. Almeida, T. C. C. França and I. Borges, *Comput. Theor. Chem.*, 2021, **1202**, 113321.

46 M. J. Frisch, G. W. Trucks, H. B. Schlegel, G. E. Scuseria, M. A. Robb, J. R. Cheeseman, G. Scalmani, V. Barone, G. A. Petersson, H. Nakatsuji, X. Li, M. Caricato, A. V. Marenich, J. Bloino, B. G. Janesko, R. Gomperts, B. Mennucci, H. P. Hratchian, J. V. Ortiz, A. F. Izmaylov, J. L. Sonnenberg, D. Williams-Young, F. Ding, F. Lipparini, F. Egidi, J. Goings, B. Peng, A. Petrone, T. Henderson, D. Ranasinghe, V. G. Zakrzewski, J. Gao, N. Rega, G. Zheng, W. Liang, M. Hada, M. Ehara, K. Toyota, R. Fukuda, J. Hasegawa, M. Ishida, T. Nakajima, Y. Honda, O. Kitao, H. Nakai, T. Vreven, K. Throssell, J. A. Montgomery, Jr., J. E. Peralta, F. Ogliaro, M. J. Bearpark, J. J. Heyd, E. N. Brothers, K. N. Kudin, V. N. Staroverov, T. A. Keith, R. Kobayashi, J. Normand, K. Raghavachari, A. P. Rendell, J. C. Burant, S. S. Iyengar, J. Tomasi, M. Cossi, J. M. Millam, M. Klene, C. Adamo, R. Cammi, J. W. Ochterski, R. L. Martin, K. Morokuma, O. Farkas, J. B. Foresman and D. J. Fox, *Gaussian 16, Revision A.03*, Wallingford CT, 2016.

47 Y. Zhao and D. G. Truhlar, *Theor. Chem. Acc.*, 2008, **120**, 215–241.

48 M. M. Franci, W. J. Pietro, W. J. Hehre, J. S. Binkley, M. S. Gordon, D. J. DeFrees and J. A. Pople, *J. Chem. Phys.*, 1982, **77**, 3654–3665.

49 T. Clark, J. Chandrasekhar, G. W. Spitznagel and P. V. R. Schleyer, *J. Comput. Chem.*, 1983, **4**, 294–301.

50 G. W. Spitznagel, T. Clark, P. von Ragué Schleyer and W. J. Hehre, *J. Comput. Chem.*, 1987, **8**, 1109–1116.

51 R. Krishnan, J. S. Binkley, R. Seeger and J. A. Pople, *J. Chem. Phys.*, 2008, **72**, 650–654.

52 A. D. McLean and G. S. Chandler, *J. Chem. Phys.*, 2008, **72**, 5639–5648.

53 K. Fukui, *Acc. Chem. Res.*, 1981, **14**, 363–368.

54 A. V. Marenich, C. J. Cramer and D. G. Truhlar, *J. Phys. Chem. B*, 2009, **113**, 6378–6396.

55 S. Grimme, J. Antony, S. Ehrlich and H. Krieg, *J. Chem. Phys.*, 2010, **132**, 154104.

56 P. J. Stephens, F. J. Devlin, C. F. Chabalowski and M. J. Frisch, *J. Phys. Chem.*, 1994, **98**, 11623–11627.

57 C. Adamo and V. Barone, *J. Chem. Phys.*, 1999, **110**, 6158–6170.

58 S. Y. Haoyu, X. He, S. L. Li and D. G. Truhlar, *Chem. Sci.*, 2016, **7**, 5032–5051.

59 J.-D. Chai and M. Head-Gordon, *Phys. Chem. Chem. Phys.*, 2008, **10**, 6615–6620.

60 F. Weigend and R. Ahlrichs, *Phys. Chem. Chem. Phys.*, 2005, **7**, 3297–3305.

61 C. Legault, *CYLview20*, 2020, <https://www.cylview.org>.

62 S. Gon Ryu and H. Wan Lee, *J. Environ. Sci. Health, Part A: Toxic/Hazard. Subst. Environ. Eng.*, 2015, **50**, 1417–1427.

63 W. M. Haynes, *CRC handbook of chemistry and physics*, CRC Press, Boca Raton, 2014.